buildings

MDPI

Article

The Vertical Behaviors of Dissimilar Pile Composite Foundations over Inclined Bedrock

Yingjie Zhou [1,3], Lihua Tan [2,3], Zhiliang Yue [2,3], Lei Yan [3], Kaiyu Jiang [3,*] and Xiaoying Gou [3,*]

[1] Chongqing Wanzhou Economic-Technological Development Area Construction & Development Co., Ltd., Chongqing 404199, China; 19123653564@163.com
[2] No. Three Engineering Co., Ltd. of CCCC First Highway Engineering Co., Ltd., Beijing 101102, China; cts0919@163.com (L.T.); 19115547884@163.com (Z.Y.)
[3] School of Civil Engineering, Chongqing Three Gorges University, Chongqing 404100, China; yanlei1988413@163.com
* Correspondence: jiangkaiyu@sanxiau.edu.cn (K.J.); xygou2017@163.com (X.G.)

Abstract: Pile composite foundations (PCFs) have been commonly applied in reinforcement engineering to adjust the vertical stiffness of foundations, due to the displacement control design criteria for foundations. PCFs that have dissimilar pile lengths, located over inclined bedrock, have shown significantly different vertical behaviors from PCFs with equal pile lengths, placed over a semi-infinite medium. However, the vertical behaviors of dissimilar PCFs over inclined bedrock cannot be predicted with the current theoretical methods, although they have been widely adopted in engineering. An analytical method is proposed in this investigation to analyze the vertical bearing characteristics of dissimilar PCFs over inclined bedrock. A pile–soil system is decomposed into fictitious piles and extended soil, and then a control equation to determine the axial force along the fictitious piles is established, stemming from the compatibility conditions between them. The vertical behaviors of dissimilar PCFs can be obtained by solving the control equation with iterative procedures, and the equation is verified by two field load tests of single piles from the Honghe bridge and a numerical case. Then, the settlement and load transfer behaviors of 3 × 1 dissimilar PCFs and their influence factors are analyzed, and the results are as follows. (1) Obvious differences can be observed concerning the axial force distribution, settlement w, and load-sharing ratio (LSR) of each pile element for different pile–soil stiffness ratios (E_p/E_s). (2) The LSR of pile 1 increases from 0.074 to 0.253 for the rigid pile and from 0.062 to 0.161 for the flexible pile condition when the cushion stiffness K_c changes from 1×10^4 kN/m to 3×10^8 kN/m. The non-dimensional vertical stiffness of the foundation, N_0/wdE_s, increases from 10.21 to 28.95 for the rigid pile condition and increases from 8.69 to 14.44 for the flexible pile condition, when K_c increases from 1×10^4 kN/m to 4×10^5 kN/m. (3) The neutral layer depth of the pile z_n, the average settlement w, and the differential settlement w_d of each element head decrease with K_c, and no negative friction zone exists (z_n = 0 m) for all the pile elements when $K_c > 2 \times 10^5$ kN/m. (4) The N_0/wdE_s decreases with the distance between the pile bottom and the inclined bedrock Δ. For the rigid and flexible pile conditions, the N_0/wdE_s is 22.16 and 13.48 for Δ = 1 m, and 13.13 and 10.10 for Δ = 8 m. The w_d reaches 16.7 mm and 4.0 mm for Δ = 1 m and Δ = 8 m, respectively. (5) The N_0/wdE_s increases almost linearly with an increase in l/d for the rigid pile condition, and it gradually decreases for the flexible pile condition. The developed model can improve the design and analysis of PCFs located over inclined bedrock under vertical loading.

Keywords: pile composite foundation; inclined bedrock; fictitious pile; dissimilar pile length; neutral layer; extended soil; cushion stiffness; load-sharing ratio

check for updates

Citation: Zhou, Y.; Tan, L.; Yue, Z.; Yan, L.; Jiang, K.; Gou, X. The Vertical Behaviors of Dissimilar Pile Composite Foundations over Inclined Bedrock. *Buildings* **2024**, *14*, 424. https://doi.org/10.3390/buildings14020424

Academic Editor: Giuseppina Uva

Received: 28 December 2023
Revised: 27 January 2024
Accepted: 29 January 2024
Published: 3 February 2024

Copyright: © 2024 by the authors. Licensee MDPI, Basel, Switzerland. This article is an open access article distributed under the terms and conditions of the Creative Commons Attribution (CC BY) license (https://creativecommons.org/licenses/by/4.0/).

1. Introduction

In the mountainous areas of China, the bedrock is often distributed non-uniformly [1–3]. For instance, a shallow buried anchorage foundation was proposed for the

Honghe bridge in Yunnan province, where the underlying stratum is inclined bedrock [4]. A pile composite foundation (PCF) with dissimilar pile lengths can significantly reduce the settlement and differential settlement of a foundation and is adopted to adjust the vertical and horizontal stiffness of a bearing stratum [5–8]. For a PCF with a dissimilar pile length over inclined bedrock, a more complex analysis is need for the key parameters, such as the penetration depth of the pile head, the load-sharing ratio (LSR) of the pile, the vertical stiffness of the PCF, and differential settlement. However, previous research has mostly focused on PCFs with equal pile lengths or on horizontally distributed bedrock [9,10], with limited reports on the vertical behavior of PCFs with dissimilar pile lengths over inclined bedrock.

Load tests [11–13] and FEM [14–16] are frequently adopted to analyze the bearing characteristics and settlement mechanisms of PCFs or pile groups in practical engineering. However, the field load test often has difficulty obtaining the ultimate loading for large pile groups or PCFs. With the design criteria of foundations shifting from bearing capacity control to displacement control in China, many analytical methods based on elasticity theory have been proposed to solve the bearing behaviors of PCFs or pile groups, such as the shear displacement method [17], load transfer method [18], simplified method [19–21], variational method [22,23], and so on. With the development of elastic methods, semi-empirical analytical methods combining the theoretical solutions of elastic methods and engineering experience coefficients have been widely applied in the current code for the design of building foundations [9] and the technical code for building pile foundations in China. The shear displacement method is not suitable to analyze the behaviors of PCFs since this method neglects vertical stress variation changes along the depth. The elastic theory proposed by Poulos cannot consider the reinforcing and shielding effects between piles and often overestimates the pile–pile or pile–soil interaction coefficients [24]. In order to reasonably consider the reinforcing and shielding effects of PCFs and pile groups, Banerjee [25], Liang [26,27], and Chen [28] have proposed integral equation methods based on the superposition principle, and Butterfield and Banerjee [29,30] and Kuwabara [31] have established rigorous boundary element methods. However, the methods mentioned above are mainly suitable for simple foundation conditions, such as a semi-infinite medium [32], or for cases in which the underlying bedrock is horizontally distributed [33]. Jiang and Hu [4,34,35] have extended the integral equation method and analyzed the behaviors of dissimilar pile rafts over inclined bedrock, but the influence of cushioning is not considered in their models. Therefore, limited research has focused on the vertical behavior of dissimilar PCFs located over inclined bedrock.

In this paper, the integral method proposed by Muki [36] is further extended to predict the vertical bearing characteristics of dissimilar PCFs over inclined bedrock. A pile–soil system is decomposed into fictitious piles and extended soil, and then a control integral equation to determine the axial force along the fictitious piles is established, stemming from the compatibility conditions between them. The vertical behaviors of dissimilar PCFs can be obtained by solving the control equation with an iterative procedure and boundary conditions. The feasibility of this method is demonstrated by two single-pile field load tests and a numerical simulation. Finally, a case study on 3×1 dissimilar PCFs is presented. Considering the LSR of the piles, the neutral layer depths of the piles, the non-dimensional vertical stiffness N_0/wdE_s, the differential settlement of the PCF w_d, and the settlement of each element top w_1 as the target parameters, the influence of some factors on the target parameters is analyzed, such as the pile–soil stiffness ratio E_p/E_s, the cushion stiffness K_c, the distance from the pile bottom to bedrock Δ, and the pile length–diameter ratio l/d. This approach is efficient and suitable for the analysis of large dissimilar PCFs.

2. Methodology

2.1. Analysis Model

A typical diagram of dissimilar PCFs located over inclined bedrock is shown in Figure 1, and the corresponding coordinate system is established. The piles are not connected to the foundation due to the existence of a cushion. There are dissimilar PCFs, including n piles with diameter d being arranged below the cushion ($n = n_1 \times n_2$), where n_1 and n_2 are the total rows and columns of piles, respectively. h_c is the cushion thickness, b is the net distance from the side pile to the foundation edge, and s is the center-to-center distance of neighboring piles. E_s, E_p, and E_c represent the elastic moduli of the soil, piles, and cushion, respectively. N_0 denotes the vertical load acting on the rigid foundation. It is assumed that the Poisson ratio of the piles, cushion, and soil is the same and it is set as v for simplicity.

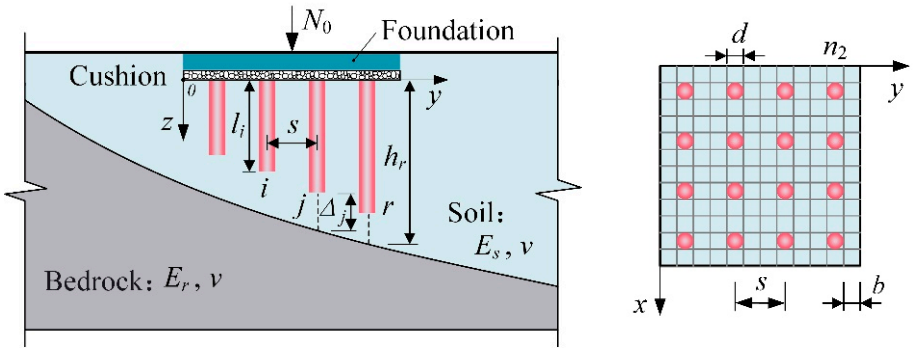


Figure 1. The dissimilar PCF system over inclined bedrock.

To investigate the interaction among the pile, soil, cushion, and foundation, the PCF system, including the cushion, is partitioned into m square units based on the pile diameter d. The pile elements have n units, and the remaining units are the soil elements. For the cushion elements, n units are connected to the rigid foundation and pile elements, and the remaining m-n units are connected to the rigid foundation and soil elements between piles. h_r denotes the bedrock-embedded depth of the r-th unit ($r = 1, 2, \ldots, m$); l_i and Δ_i are the length of pile i and the distance from the pile bottom to the bedrock of pile i ($i = 1, 2, \ldots, n$). Therefore, for the i-th pile unit, it is $h_i = l_i + \Delta_i$.

The cushion layer can be regarded as a spring system connecting the PCF system with the rigid foundation. The vertical loads acting at the i-th pile head and k-th soil unit head are illustrated as $P^i(0)$ and $Q^k(0)$ ($i = 1, 2, \ldots, n$; $k = n + 1, n + 2, \ldots, m$), respectively, as shown in Figure 2.

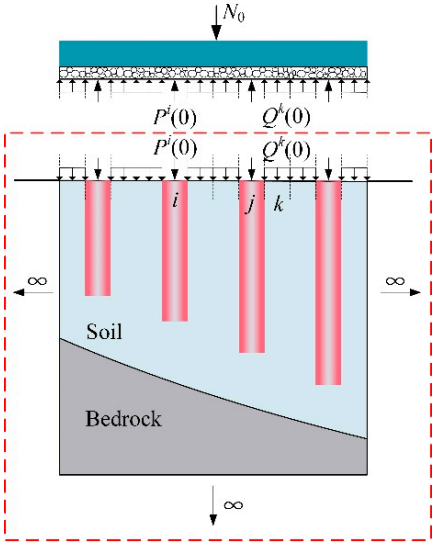


Figure 2. Load distribution for the bottom of the cushion.

Following the method proposed by Muki, the pile–soil system can be further decomposed into fictitious piles and extended soil (Figure 3). $P_*^i(z)$ and $q^i(z)$, respectively, represent the axial force and shaft resistance of the i-th fictitious pile at a depth of z. For instance, $P_*^i(0)$ and $P_*^i(l_i)$ are the axial forces on the head and bottom of the i-th fictitious pile. The force analysis diagram of the extended soil can be obtained as shown in Figure 3 based on the principles of action and reaction.

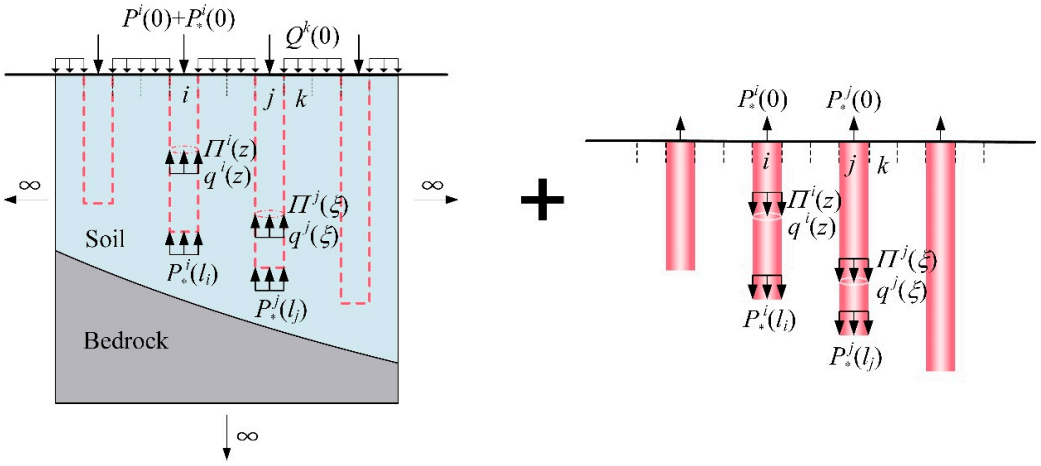


Figure 3. Decomposition for pile–soil system.

2.2. Cushion

The m cushion units are assumed to be ideal isotropic cylinders, the diameters are the same as those of the piles, and the self-weight and shaft friction of the cylinders can be neglected.

For the cushion unit above the i-th fictitious pile, the compression, s_c^i, can be obtained based on the generalized Hooke's law as follows:

$$s_c^i = \int_0^{h_c} \varepsilon_c^i dh = \frac{h_c}{E_c}\left(\sigma_{cz}^i - 2\nu\sigma_{ch}^i\right)(i = 1,\ 2,\ \ldots, n) \tag{1}$$

For the i-th cushion unit, the vertical stress is the principal factor. Supposing that α_i is the ratio of radial strain to vertical strain under triaxial compression conditions, the lateral pressure coefficient can be expressed as

$$k_{lateral}^i = \frac{\nu + \alpha_i}{1 - \nu + 2\nu\alpha_i}(i = 1,\ 2,\ \ldots, n) \tag{2}$$

Combining Equations (1) and (2), the vertical stiffness of the i-th cushion unit can be calculated as shown in Equation (3).

$$K_c^i = \frac{1 - \nu + 2\nu\alpha_i}{(1+\nu)(1-2\nu)}\frac{E_c A}{h_c}\ (i = 1, 2, \ldots, n) \tag{3}$$

where A represents the cross-sectional area of the cushion unit.

Similarly, for the cushion unit above the k-th soil unit, suppose that β_k is the ratio of radial strain to vertical strain under triaxial compression conditions. Then, the vertical stiffness of the k-th cushion unit can be calculated as follows:

$$K_c^k = \frac{1 - \nu + 2\nu\beta_k}{(1+\nu)(1-2\nu)}\frac{E_c A}{h_c}\ (k = n+1, n+2, \ldots, m) \tag{4}$$

α_i and β_k can be determined from the same radial stress condition as the neighboring units. The pile head penetration effect can be calculated by analyzing the compression of each cushion unit above the pile and soil units, and the pile bottom penetration effect can also be considered by analyzing the compression of each pile and soil unit at the pile bottom depth.

2.3. Fictitious Pile

For the *i*-th fictitious pile, the vertical stress–strain relationship, the equilibrium condition of the micro-element, and the vertical strain–settlement relationship can be expressed as follows:

$$\varepsilon_*^i(z) = \frac{P_*^i(z)}{E_* A}(0 \ \le z \le l_i, i = 1,\ 2, \ldots, n) \tag{5}$$

$$\frac{dP_*^i(z)}{dz} = -q^i(z)(0 \ \le z \le l_i, i = 1,\ 2, \ldots, n) \tag{6}$$

$$\varepsilon_*^i(z) = \frac{dw_*^i(z)}{dz}(0 \ \le z \le l_i, i = 1,\ 2, \ldots, n) \tag{7}$$

where $\varepsilon_*^i(z)$, $w_*^i(z)$, and A, respectively, represent the vertical strain, the settlement at the depth of z, and the cross-sectional area of the fictitious pile. E_* denotes the Young's modulus of fictitious pile elements, and it can be expressed as $E_* = E_p - E_s$.

The settlement of the *i*-th fictitious pile at depth z can be determined as follows:

$$w_*^i(z) = w_*^i(0) + \int_0^z \frac{P_*^i(\xi)}{E_*^i A} d\xi \ (0 \ \le z \le l_i, i = 1,\ 2, \ldots, n) \tag{8}$$

where $w_*^i(0)$ is the pile head settlement for the *i*-th fictitious pile.

2.4. Extended Soil

For the *r*-th extended soil (r = 1, 2,. . ., m), the vertical stress of $\sigma_z^r(z)$, the vertical strain of $\varepsilon_z^r(z)$, and the settlement of $w_z^r(z)$ at the depth of z can be expressed by the superposition principle as follows:

$$\sigma_z^r(z) = \sum_{j=1}^{n} \left\{ \begin{array}{l} \left[P^j(0) + P_*^j(0)\right]\sigma_z^{rj}(z,0) \\ -P_*^j(l_j)\sigma_z^{rj}(z,l_j) - \int_0^{l_j} q^j(\xi)\sigma_z^{rj}(z,\xi)d\xi \end{array} \right\} + \sum_{k=n+1}^{m} Q^k(0)\sigma_z^{rk}(z,0) \qquad (0 \le z \le h_r) \tag{9}$$

$$\varepsilon_z^r(z) = \sum_{j=1}^{n} \left\{ \begin{array}{l} \left[P^j(0) + P_*^j(0)\right]\varepsilon_z^{rj}(z,0) \\ -P_*^j(l_j)\varepsilon_z^{rj}(z,l_j) - \int_0^{l_j} q^j(\xi)\varepsilon_z^{rj}(z,\xi)d\xi \end{array} \right\} + \sum_{k=n+1}^{m} Q^k(0)\varepsilon_z^{rk}(z,0) \qquad (0 \le z \le h_r) \tag{10}$$

$$w_z^r(z) = \sum_{j=1}^{n} \left\{ \begin{array}{l} \left[P^j(0) + P_*^j(0)\right]w_z^{rj}(z,0) \\ -P_*^j(l_j)w_z^{rj}(z,l_j) - \int_0^{l_j} q^j(\xi)w_z^{rj}(z,\xi)d\xi \end{array} \right\} + \sum_{k=n+1}^{m} Q^k(0)w_z^{rk}(z,0) \qquad (0 \le z \le h_r) \tag{11}$$

For the uniform distribution and unit vertical load at region $\Pi(\xi)$ of the *j*-th extended soil, $\sigma_z^{rj}(z,\xi)$, $\varepsilon_z^{rj}(z,\xi)$, and $w_z^{rj}(z,\xi)$, respectively, represent the influence coefficients of the average vertical stress, vertical strain, and settlement of the *r*-th extended soil at the depth of z. For the uniform distribution and unit vertical load at region $\Pi(0)$ of the *k*-th extended soil, $\sigma_z^{rk}(z,0)$, $\varepsilon_z^{rk}(z,0)$, and $w_z^{rk}(z,0)$, respectively, denote the influence coefficients of the average vertical stress, vertical strain, and settlement of the *r*-th extended soil at the depth of z.

The theoretical solution for the stress and settlement of a layered elastic foundation is crucial for foundation design and application. The solutions for the vertical stress and settlement of two horizontally layered foundations were derived by Burmister [37]. Based on the Steinbrenner approximation method, Kitiyodom [38] proposed a modified Mindlin

solution [37] and applied it to analyze the pile raft foundation. For an elastic medium with a rough, rigid layer, Poulos [39] derived the numerical solution of the corresponding stresses and displacements. When comparing Poulos's solutions to the corresponding solutions of the semi-infinite medium condition, a negligible discrepancy can be observed at a large depth when Poisson's ratio v = 0.5. More importantly, the analytic solutions for the stress and displacement of layered elastic media often involve the integration of Bessel functions, which is inconvenient for engineering applications. In the complex interaction between the bedrock and soil medium, the theoretical analytic solutions of stress and displacement for the inclined bedrock condition cannot be observed. Therefore, the vertical stress and settlement influence coefficients are expressed by integrating Mindlin's solutions for simplification. Moreover, the vertical strain influence coefficient can be determined by the settlement influence solution.

When $z = \xi$, considering the finite jump characteristics of $\sigma_z^{ii}(z,\xi)$ and $\varepsilon_z^{ii}(z,\xi)$, $\sigma_z^{rj}(z,\xi)$, $\varepsilon_z^{rj}(z,\xi)$, and $w_z^{rj}(z,\xi)$ can be further derived by integration, combining Equations (6) and (12)–(14).

$$\sigma_z^r(z) = P_*^i(z)\left[\sigma_z^{ii}(z,z^-) - \sigma_z^{ii}(z,z^+)\right] - \sum_{j=1}^{n}\int_0^{l_j} P_*^j(\xi)\frac{\partial\sigma_z^{rj}(z,\xi)}{\partial\xi}d\xi + \sum_{j=1}^{n} P^j(0)\sigma_z^{rj}(z,0) + \sum_{k=n+1}^{m} Q^k(0)\sigma_z^{rk}(z,0) \quad (12)$$

$$\varepsilon_z^r(z) = P_*^i(z)\left[\varepsilon_z^{ii}(z,z^-) - \varepsilon_z^{ii}(z,z^+)\right] - \sum_{j=1}^{n}\int_0^{l_j} P_*^j(\xi)\frac{\partial\varepsilon_z^{rj}(z,\xi)}{\partial\xi}d\xi + \sum_{j=1}^{n} P^j(0)\varepsilon_z^{rj}(z,0) + \sum_{k=n+1}^{m} Q^k(0)\varepsilon_z^{rk}(z,0) \quad (13)$$

$$w_s^r(z) = -\sum_{j=1}^{n}\int_0^{l_j} P_*^j(\xi)\frac{\partial w_z^{rj}(z,\xi)}{\partial\xi}d\xi + \sum_{j=1}^{n} P^j(0)w_z^{rj}(z,0) + \sum_{k=n+1}^{m} Q^k(0)w_z^{rk}(z,0) \quad (14)$$

Based on Hooke's law and equilibrium conditions, we have $\varepsilon_z^{ii}(z,z^+) - \varepsilon_z^{ii}(z,z^-) = \frac{(2v-1)(1+v)}{E_s A(1-v)}$, $\sigma_z^{ii}(z,z^+) - \sigma_z^{ii}(z,z^-) = -1/A$.

2.5. Governing Integral Equations

Based on the vertical strain compatibility condition, we can establish the governing integral equation at the same depth between the extended soil and fictitious piles.

$$\left[-\frac{1}{E_*} - \frac{(1-2v)(1+v)}{E_s(1-v)}\right]P_*^i(z) + A\sum_{j=1}^{n}\int_0^{l_j} P_*^i(\xi)\frac{\partial\varepsilon_z^{ij}(z,\xi)}{\partial\xi}d\xi = A\left(\sum_{j=1}^{n} P^j(0)\varepsilon_z^{ij}(z,0) + \sum_{k=n+1}^{m} Q^k(0)\varepsilon_z^{ik}(z,0)\right) \quad (15)$$

Equation (15) is known as the Fredholm integral equation of the second kind regarding the axial forces of fictitious piles. Moreover, there are two typical foundation conditions.

(1) Flexible foundation condition

For the flexible foundation, the governing Equation (15) can be directly solved as the known load of each element top. Therefore, the axial force of each fictitious pile $P_*^i(z)$ (i = 1, 2,. . ., n) can directly be obtained, and the axial forces $P^r(z)$ and settlement $W^r(z)$ (r = 1, 2,. . ., m) of the actual pile and soil elements also can be determined by superposing the axial force of the r-th fictitious pile and the vertical force of the r-th extended soil element $\sigma_z^r(z)A$, as shown in Equation (16).

$$P^r(z) = -A\sum_{j=1}^{n}\int_0^{l_j} P_*^j(\xi)\frac{\partial\sigma_z^{rj}(z,\xi)}{\partial\xi}d\xi + A\sum_{j=1}^{n} P^j(0)\sigma_z^{rj}(z,0) + A\sum_{k=n+1}^{m} Q^k(0)\sigma_z^{rk}(z,0) \quad (16)$$

where $P^r(z)$ is assumed to be positive under the compression condition, and the axial load of the r-th actual element head $P^r(0)$ can be obtained when $z = 0$ in Equation (16).

The settlement of the i-th fictitious pile $w_p^i(z)$ at depth z is coincident with the extended soil in the corresponding position $w_s^r(z)$. For instance, when $r = i$, we have

$$w_p^i(z) = w_s^r(z)(r = i) \tag{17}$$

As mentioned above, h_r denotes the bedrock-embedded depth of the r-th unit. It is reasonable to suppose that the bedrock surface of each unit has no settlement. Therefore, the actual settlement for the r-th element with a finite depth h_r can be expressed as

$$W^r(z) = w_s^r(z) - w_s^r(h_r) \tag{18}$$

Under the condition of $z = 0$, the settlement of each element head can be obtained.

(2) Rigid foundation condition

For the rigid foundation condition, the governing Equation (15) cannot be directly solved due to the unknown vertical load of each element head. Therefore, additional deformation compatibility conditions and equilibrium equations must be introduced.

The vertical stiffness of the dissimilar PCF system over inclined bedrock obviously shows a non-uniform distribution. Therefore, the average settlement w and inclination slope θ of a rigid foundation should be compatible with the settlement of the corresponding cushion element head. For instance, the compression of the r-th cushion element s_c^r, the settlement of the r-th sub-element head $W^r(0)$, and the settlement of the rigid foundation at the corresponding position should be compatible, as shown in below.

$$W^r(0) + s_c^r = w + \theta\Omega \ (r = 1,\ 2, \ldots, m) \tag{19}$$

Based on the equilibrium conditions of a rigid foundation, we have

$$N_0 = \sum_{i=1}^{n} P_p^i(0) + \sum_{k=n+1}^{m} Q^k(0) \ (i = 1,\ 2, \ldots, n; k = n+1, n+2, \ldots, m) \tag{20}$$

where Ω is the position coordinate matrix about each sub-element, which can be obtained from the coordinate system in Figure 1.

Combining Equations (15), (19) and (20), the axial forces of all the fictitious piles can be achieved; furthermore, the axial forces and settlement of each actual pile element and soil element along the depth can be obtained. Then, the compression of each cushion element, the pile–soil stress sharing ratio, and the pile shaft friction can be analyzed.

In particular, once the vertical load P (0) and settlement $W^r(0)$ of the r-th sub-element head are determined, the vertical stiffness $K^r(0)$ of the r-th sub-element head can be calculated as follows:

$$K^r(0) = \frac{P^r(0)}{W^r(0) + s_c^r} \tag{21}$$

2.6. Numerical Solution

Calculating the governing Equation (15) is the key step for a reasonable result.

Equation (15) can be solved by the numerical integration method due to its simplicity and ease, which transforms the integral equation into an algebraic equation. The basic process is illustrated in Figure 4.

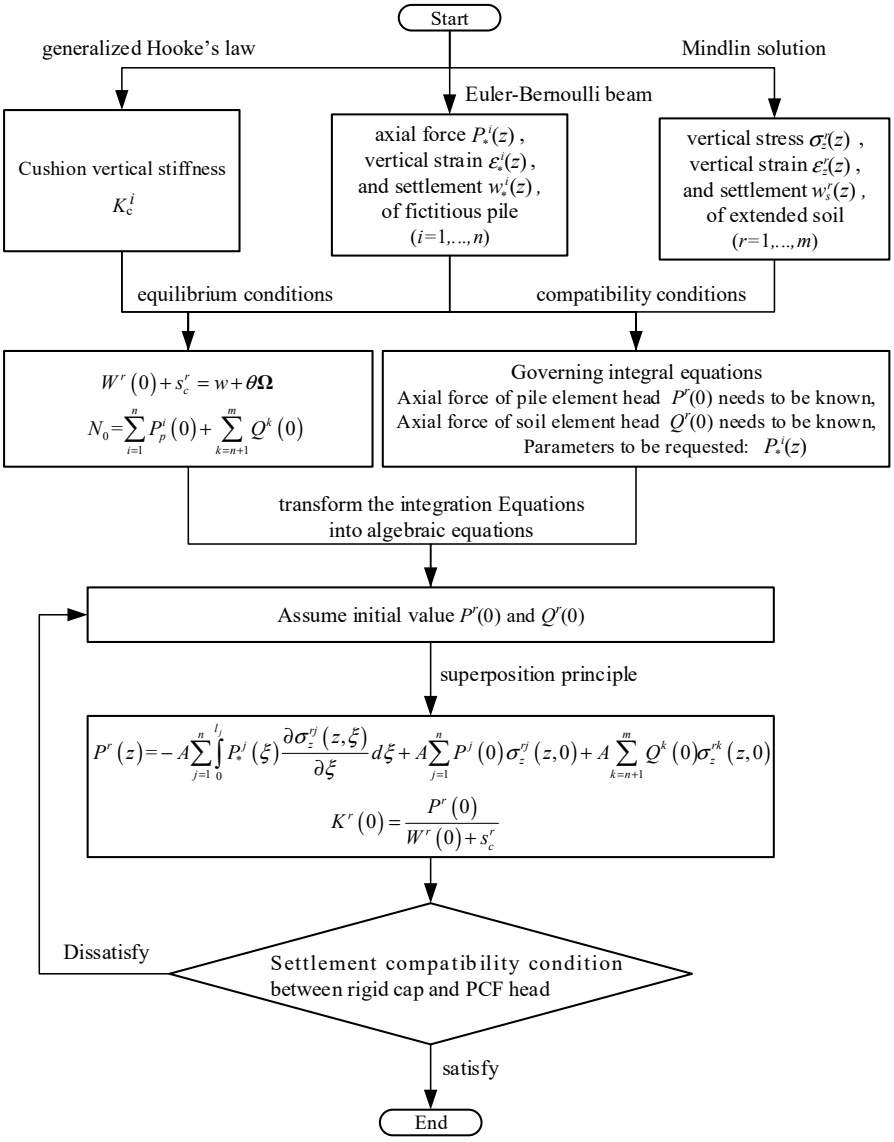


Figure 4. Basic solution process combining iteration algorithm.

3. Validation of Proposed Method

To validate the accuracy of the proposed method, we carry out two single pile field load tests and an FEM case.

3.1. Two Single Pile Field Load Tests

A shallow buried anchorage foundation is located in Honghe bridge in Yunnan province, where the underlying stratum is inclined bedrock. The bottom size of the foundation is 48 × 62 m. The back and front areas of the foundation are located over moderately weathered slate and strongly weathered slate, respectively. As shown in Figure 5, a dissimilar rigid PCF is adopted to adjust the vertical and horizontal stiffness of the bearing stratum. The rigid piles are arranged in a rectangular layout to enhance the strongly weathered slate. The load tests for two single piles are investigated and indicated by the 7th row in Figure 5. The diameter, pile spacing, and length of the loaded two piles are, respectively, 1.2 m, 4.5 m, and 9.4 m. The elastic modulus of the pile and strongly weathered slate are supposed to be 300 MPa and 30 GPa. The Poisson ratio is 0.25 for the pile and strongly weathered slate.

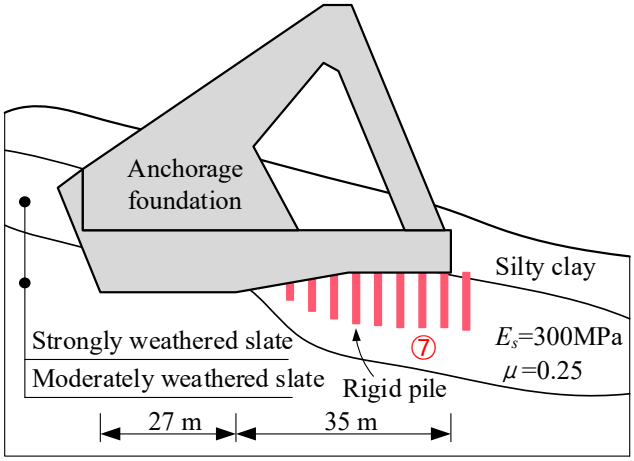


Figure 5. Schematic diagram of the shallow buried anchorage foundation.

Figure 6 depicts the *Q*–*s* curves of the two load tests and theoretical solutions, and the initial stages are similar. The *Q*–*s* curves present a line distribution because the soil is in an elastic state at the initial loading process, and the theoretical method is suitable for elasticity analysis. When the loading increases, a significant difference in the *Q*–*s* curves between the two methods can be observed when the plastic settlement emerges [40]. In practical engineering, the ground is often in an elastic state, and the design criteria of the foundation have shifted from bearing capacity control to displacement control in China, which means that the theoretical method is suitable for analyzing PCFs. Comparing the theoretical solutions, the enforcement and shielding effects of neighborhood piles offer limited improvements in the pile stiffness on the condition of the large pile spacing.

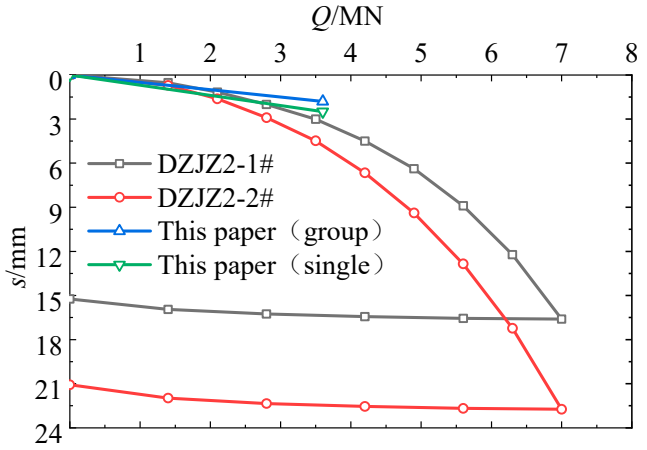


Figure 6. *Q*–*s* curves of field tests and theoretical method.

3.2. Vertically Loaded 3 × 1 Dissimilar PCF

For further verify the feasibility of this theoretical method, the vertical behaviors of a 3 × 1 dissimilar PCF are also analyzed with FEM. The configuration and parameters of the 3 × 1 dissimilar PCF over the soil–rock composite ground is illustrated in Figure 7.

The axial force and settlement distribution along the pile shafts of piles 2 and 3 are presented in Figure 8. It can be observed that the results of the proposed method match the FEM solutions reasonably. The accuracy of the theoretical method is related to the length of the sub-element, and the solution accuracy of FEM can also be affected by the mesh size. Therefore, the results of the two methods are not completely consistent. Following the two cases' validation above, the proposed method is reliable.

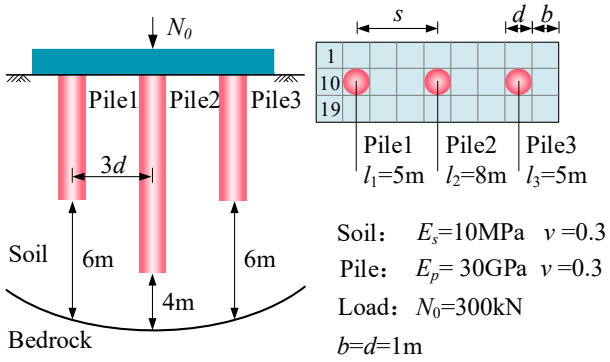


Figure 7. The 3 × 1 dissimilar PCF and corresponding parameters.

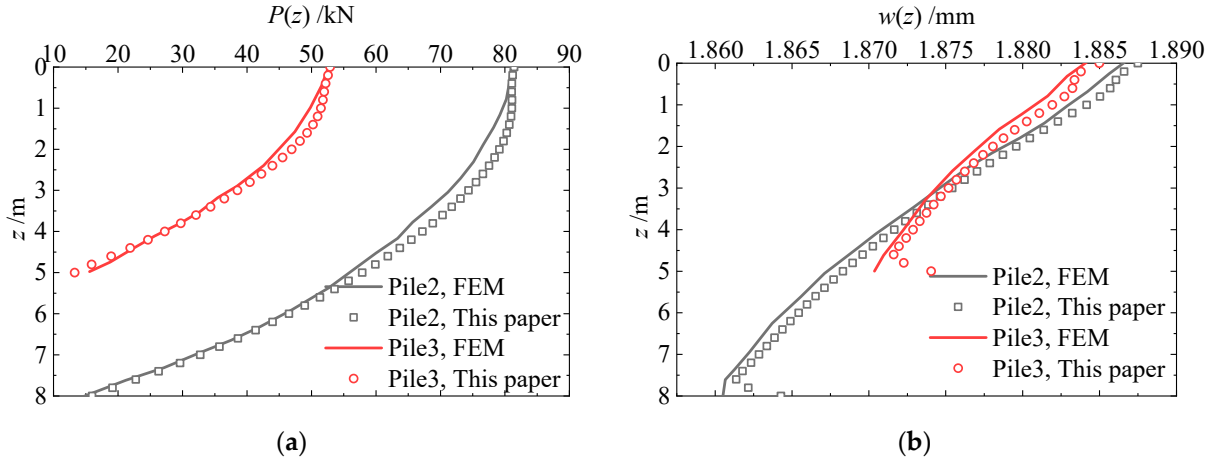


Figure 8. Axial force and settlement distribution. (**a**) Axial force distribution of piles. (**b**) Settlement distribution of piles.

4. Case Study

A vertically loaded 3 × 1 dissimilar PCF with a rigid cap over inclined bedrock is studied, and the parameters of the PCFs [41] and soil are illustrated in Figure 9. The influence of the cushion, inclined bedrock, pile rigidity, and length to diameter ratio of the pile on the bearing characteristics and deformation mechanism of the PCF is the main target.

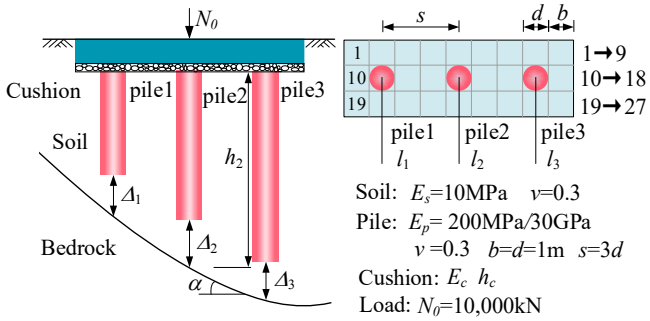


Figure 9. The 3 × 1 dissimilar PCF with cushion.

4.1. Vertical Bearing Behaviors

The underlying bedrock is modeled as an inclined plane and is perpendicular to the *oyz* plane. The inclined angle of bedrock $\alpha = 30°$, and $E_c = 50$ MPa and $h_c = 0.5$ m; the length of pile 2 $l_2 = 8$ m. Δ_i ($i = 1, 2, 3$) are assumed to be the same, and $\Delta = 1$ m is set for simplicity. The PCF system, including the cushion, is divided into 27 square elements based on the

pile diameter d. The length of pile 1 and pile 3 can be obtained using the pile spacing s and inclination angle α, whereas the embedded depth of the bedrock for each element can be determined from pile length l and Δ.

The axial force distribution of typical units is shown in Figures 10 and 11. It can be seen that (1) negative friction near the pile head always exists for all the pile elements with the presence of the cushion. The axial force of the pile element increases initially and then decreases along the pile shaft, and the neutral point of the pile shaft is at about z = 1.2 m. (2) The axial force of soil element 12 is significantly smaller than that of the pile elements and decreases with depth. (3) Regarding the axial force at the same depth for the rigid pile condition, we have the following: pile 3 (long pile) > pile 2 > pile 1 (short pile). For the flexible pile condition, we have pile 3 (long pile) > pile 2> pile 1 (short pile) when z = 0~2.4 m, and pile 3 (long pile) > pile 2 > pile 1 (short pile) when z > 2.4 m. The axial force distribution law has shown that the pile length plays a controlling role in LSR as piles have strong load transfer abilities for the rigid pile condition. Therefore, the axial force of the pile increases with the pile length. However, for the flexible pile condition, the LSR of the piles is not only affected by the pile length but also by the parameter Δ due to its relatively weak load transfer ability. Although the length of pile 1 is shorter than that of pile 2, the LSR of pile 1 is still larger than that of pile 2 when synthetically considering the influence of parameter Δ. (4) The LSR in the flexible pile condition is significantly smaller than in the rigid pile condition.

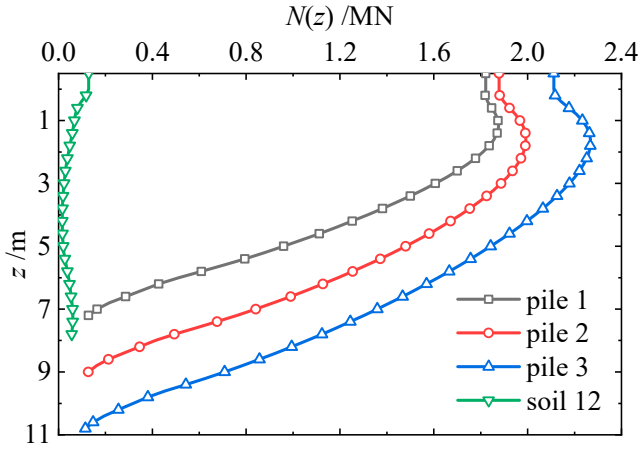


Figure 10. Axial force distribution for rigid pile.

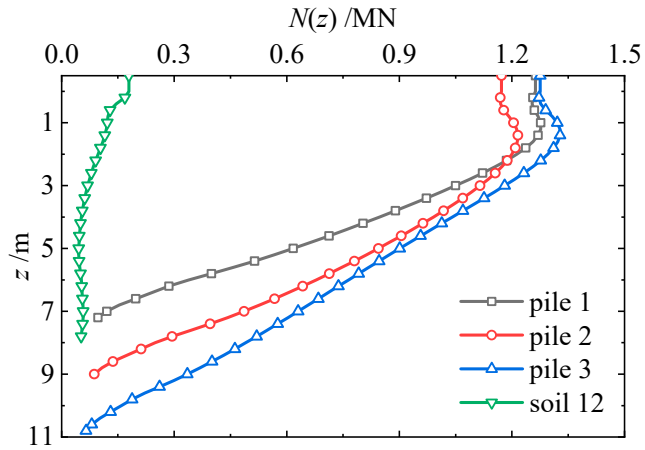


Figure 11. Axial force distribution for flexible pile.

Soil element 12 is the neighboring unit between pile 1 and pile 2. The settlement distribution of the pile elements and soil element 12 for different pile rigidity conditions is depicted in Figures 12 and 13. It can be observed that (1) for the rigid pile condition, the

compression of the pile elements is relatively small at about 1 mm, which indicates a rigid body deformation mode. For the settlement of the piles, we have pile 1 > pile 2 > pile 3, and counterclockwise rotation has been generated. The settlement of soil element 12 is larger than that of the pile elements near the surface and decreases rapidly with depth. The neutral point is located at z = 3 m. (2) For the flexible pile condition, the settlement of all the elements is significantly larger than in the rigid pile condition, and the compression of the pile shaft cannot be ignored. For instance, the compression of pile 1, pile 2, and pile 3 is 37 mm, 46 mm, and 55 mm, respectively. The settlement of soil element 12 is approximately equal to that of the piles, and the depths of the neutral points of the piles present notable differences. For instance, the depth of the neutral point of pile 1, pile 2, and pile 3 is 4 m, 1.6 m, and 0.4 m, respectively.

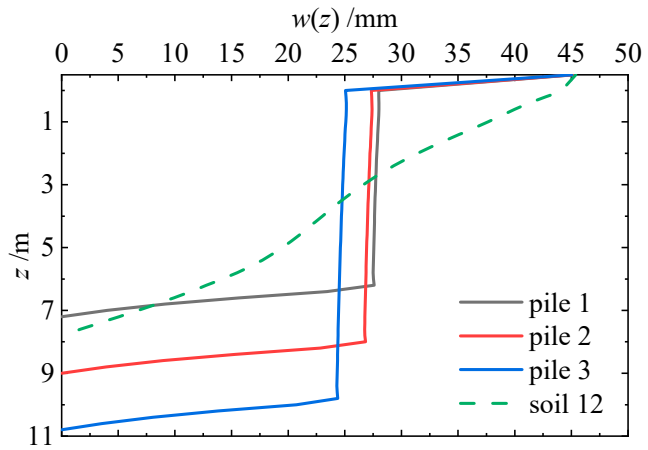


Figure 12. Settlement distribution for the rigid pile.

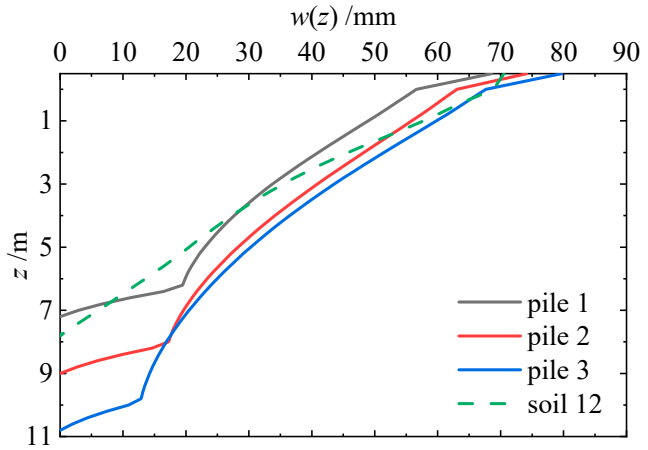


Figure 13. Settlement distribution for the flexible pile.

The LSRs of each element for the two pile rigidity conditions are illustrated in Figure 14. The LSR of the pile to soil elements for the rigid pile condition is much larger than that in the flexible pile condition, and the LSRs of the pile to soil elements are 0.58 and 0.37 for the two pile rigidity conditions, respectively. The LSRs of pile 1 to the neighboring soil element 12 are 14.2 and 7.1 for the two pile rigidity conditions, respectively, which shows that the pile rigidity has a significant effect on the LSR of the PCF.

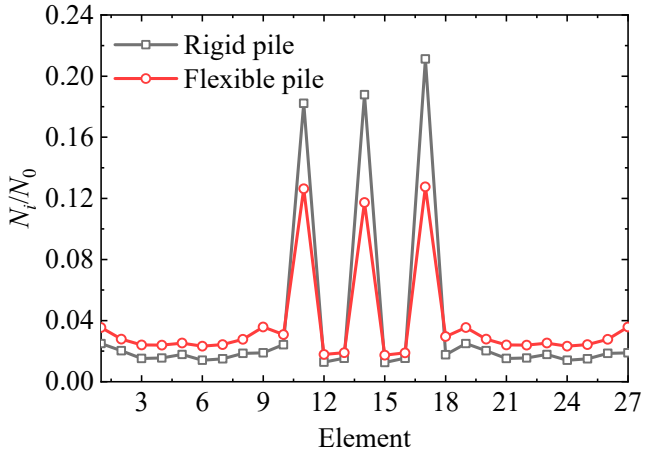


Figure 14. The LSRs of each element.

4.2. Cushion Stiffness Effect

The effect of cushion stiffness K_c on the PCF proposed in Figure 9 is investigated. In this part, the range of K_c is set from 1×10^4 kN/m~3×10^8 kN/m, which covers the range of cushion stiffness for major practical applications [42–44]. The remaining parameters are still identified before each case.

The variations in the neutral layer depth of the pile elements with K_c are illustrated in Figures 15 and 16. It can be obtained that (1) the neutral layer depths for all the pile elements gradually decrease with the increase in cushion stiffness until 0 m, which indicates that the regions of negative friction near the pile head decrease and disappear with the increasing cushion stiffness. (2) For the rigid pile condition, the neutral layer depths of pile 1, pile 2, and pile 3 are 2.2 m, 2.8 m, and 3.0 m, respectively, when $K_c = 1 \times 10^4$ kN/m, and 0 m, 1.0 m, and 1.2 m when $K_c = 2 \times 10^5$ kN/m. Zhang [40] has proposed that negative friction often occurs within one quarter of the pile length for the PCF by FEM, which is consistent with the theoretical solution. No negative friction zone exists for all the pile elements when $K_c > 2 \times 10^5$ kN/m. (3) For the flexible pile condition, the neutral layer depths of pile 1, pile 2, and pile 3 are 2.0 m, 2.4 m, and 2.2 m, respectively, when $K_c = 1 \times 10^4$ kN/m, and 0 m, 0 m, and 1.0 m when $K_c = 2 \times 10^5$ kN/m. No negative friction zone exists for all the pile elements when $K_c > 2 \times 10^5$ kN/m. (4) The neutral layer depth of the piles for the rigid pile condition is larger than that in the flexible pile condition. Therefore, K_c has a notable effect on the depth of the neutral layer and the vertical behaviors of the PCF.

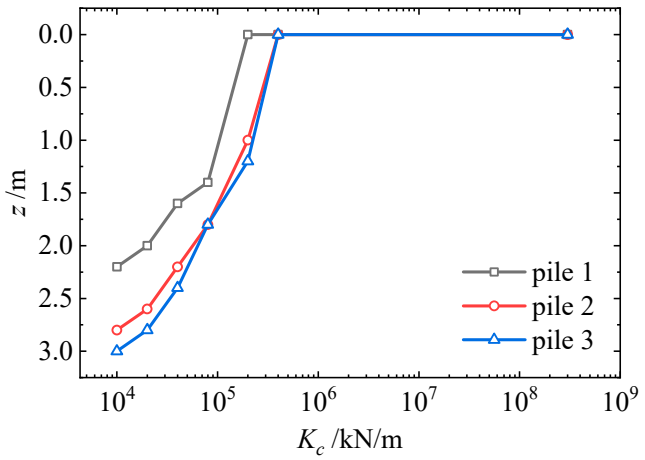


Figure 15. Neutral layer depth for rigid pile.

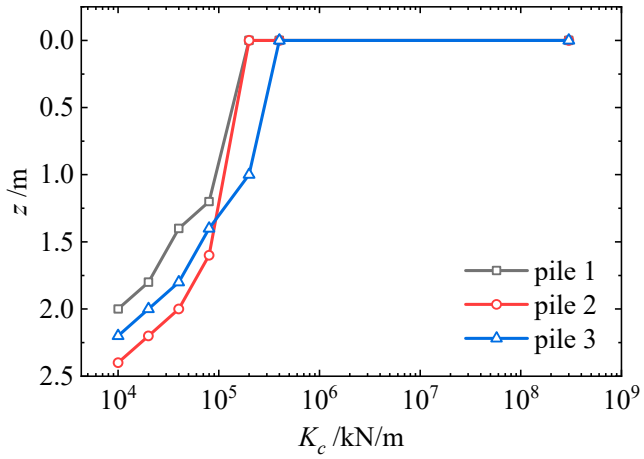


Figure 16. Neutral layer depth for flexible pile.

The LSRs of each element for the two pile rigidity conditions are shown in Figures 17 and 18. The horizontal axis represents the element number, following the numbering convention in Figure 18, and the vertical axis represents the ratio of the axial force of each element head to the vertical load N_0. It can be concluded that (1) stress concentration exists as the vertical stiffness of the pile elements is significantly greater than that of the soil elements, and the stress concentration value increases with the cushion stiffness. When K_c changes from 1×10^4 kN/m to 3×10^8 kN/m, the LSR of pile 1 increases from 0.074 to 0.253 for the rigid pile condition, and from 0.062 to 0.161 for the flexible pile condition. (2) For the rigid pile condition, the LSR of pile 3 exhibits the fastest growth with K_c as the length of pile 3 is the longest among all piles. Similarly, the LSR of pile 2 is slightly larger than that of pile 1 due to the relation of the pile length. (3) For flexible pile conditions, the LSRs of the piles are significantly affected by the pile length and the buried depth of the bedrock. The vertical stiffness of pile 1 and pile 3 does not show notable differences, due to the shorter pile length and smaller buried depth of the bedrock for pile 1 and vice versa for pile 3.

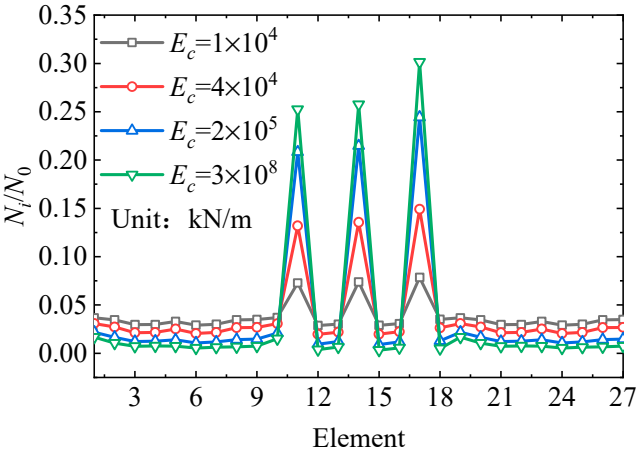


Figure 17. The LSRs for rigid pile condition.

Figure 19 illustrates the relationship between the N_0/wdE_s of the PCF and K_c. We have the following results. (1) The N_0/wdE_s increases with the increase in K_c for the two pile rigidity conditions, and a more notable increase can be observed for the rigid pile condition. For instance, when K_c increases from 1×10^4 kN/m to 4×10^5 kN/m, the N_0/wdE_s increases from 10.21 to 28.95 for the rigid pile condition, and it increases from 8.69 to 14.44 for the flexible pile condition. (2) The N_0/wdE_s presents a relatively slow increase when $K_c > 4 \times 10^5$ kN/m. The K_c value increases about 750 times when

K_c increases from 4×10^5 kN/m to 3×10^8 kN/m, but the N_0/wdE_s only increases from 28.95 to 34.09 for the rigid pile condition and 14.44 to 14.88 for the flexible pile condition.

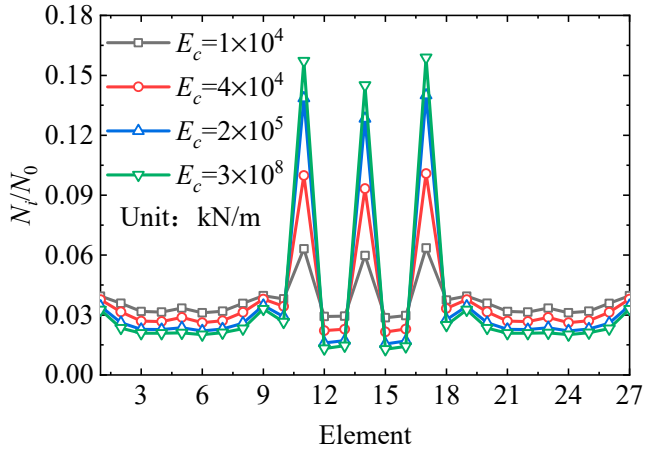


Figure 18. The LSRs for flexible pile condition.

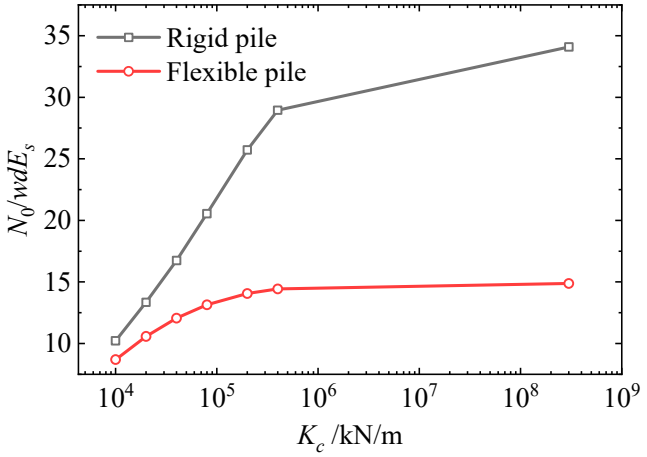


Figure 19. The relationship of N_0/wdE_s and K_c.

The variation for the differential settlement of rigid foundation w_d is shown in Figure 20, considering different values of K_c and pile rigidity. According to the coordinate system defined in Figure 1, the sign of w_d is negative when the rigid foundation experiences counterclockwise rotation, and vice versa.

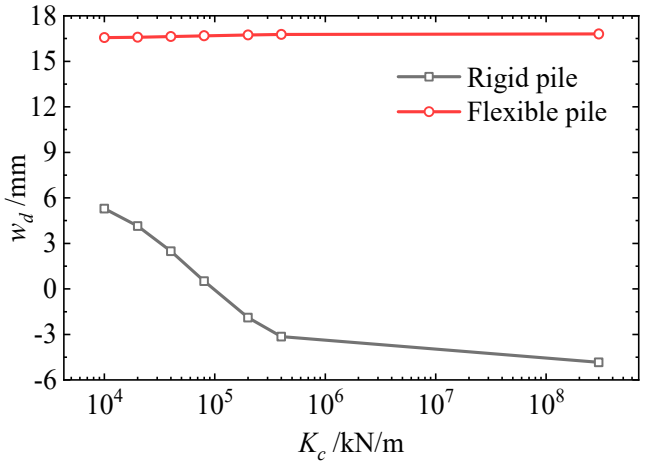


Figure 20. The differential settlement w_d of foundation.

For the rigid pile condition, the sign of w_d gradually decreases from positive to negative with the increase in K_c. This means that the settlement of pile 3 is larger than that of pile 1 for the smaller K_c condition, and, conversely, the settlement of pile 3 is smaller than that of pile 1 for the larger K_c condition. For instance, the differential settlement of rigid foundation w_d = 5.29 mm when $K_c = 1 \times 10^4$ kN/m, and $w_d = -4.84$ mm when $K_c = 3 \times 10^8$ kN/m. Therefore, K_c has a significant influence on the differential settlement of rigid foundation w_d.

For the flexible pile condition, the differential settlement of rigid foundation w_d almost remains constant for different values of K_c, and the sign of w_d is always positive. The rigid foundation presents clockwise rotation consistently, and the value of w_d falls between 16.56 mm and 16.80 mm. It can be concluded that the buried depth of the bedrock has a controlling effect as the settlement of the longer pile (pile 3) is larger than that of the shorter pile (pile 1) considering the existence of inclined bedrock.

The distribution of settlement for each element head w_1 for different pile rigidity conditions is illustrated in Figures 21 and 22, respectively. It can be observed that (1) the settlements of each element head w_1 gradually decrease with the K_c increase; (2) the average settlement and differential settlement of the rigid foundation gradually decrease with K_c; (3) the settlement of the rigid foundation is consistent with the settlement of each element head, as no compression exists for cushion elements when $K_c = 3 \times 10^8$ kN/m.

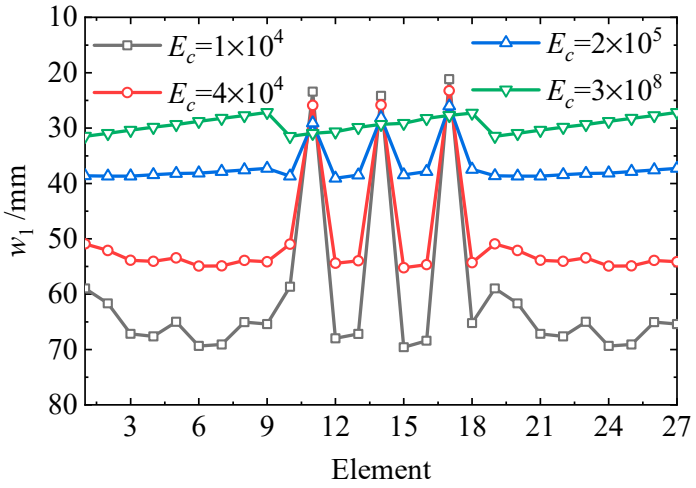


Figure 21. The settlement of pile and soil element head (rigid pile).

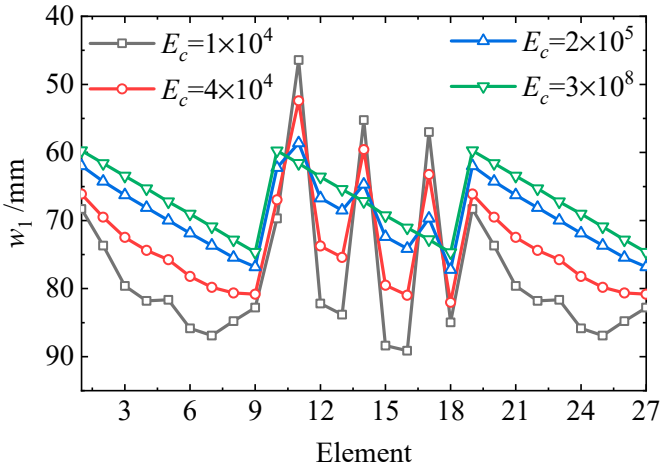


Figure 22. The settlement of pile and soil element head (flexible pile).

4.3. Effect of Distance from Pile Bottom to Bedrock Δ

The influence of Δ on the bearing behaviors of the PCF proposed in Figure 9 is illustrated. In this part, the range of Δ/*d* is set from 1 to 8, and the remaining parameters are still in line with previous configurations. It is mentioned that the underlying bedrock has no impact on the PCF when $\Delta/d \geq 8$ when combining engineering experience. Therefore, the foundation can be regarded as a semi-infinite elastic medium when $\Delta/d \geq 8$.

Figures 23 and 24 illustrate the relationship between the neutral layer depth of each pile element and Δ for the two pile rigidity conditions, respectively, and they show that Δ has little effect on the neutral layer depth of the piles. For the rigid pile condition, the neutral layer depth is between 1.2 and 1.4 m for pile 1, and between 1.6 and 2.0 m for pile 2 and pile 3. For the flexible pile condition, the neutral layer depth remains constant with different Δ for all the pile elements, except the condition of Δ = 1 m for pile 2. The neutral layer depths of pile 1, pile 2, and pile 3 are 1.2 m, 1.4 m, and 1.6 m, respectively. Moreover, the neutral layer depth of pile 1 is the smallest, and the neutral layer depth for the flexible pile condition is smaller than that of the rigid pile condition for the same Δ.

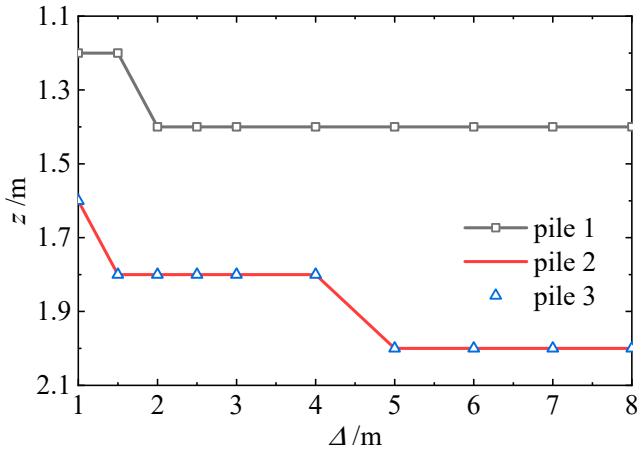


Figure 23. Neutral layer depth for rigid pile.

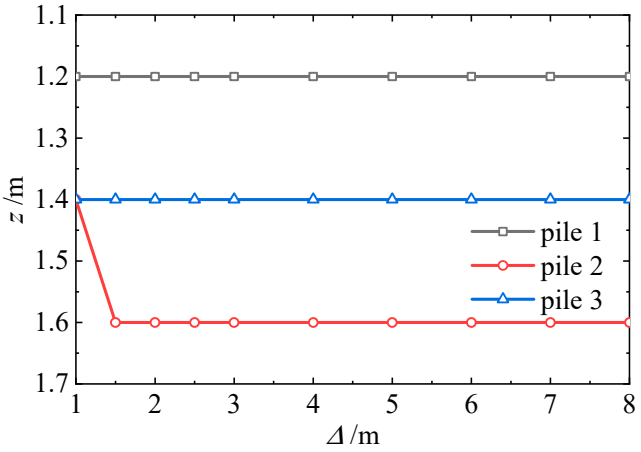


Figure 24. Neutral layer depth for flexible pile.

The LSR of the pile to soil decreases with Δ, as the increase in Δ weakens the relative stiffness of the pile to soil. Therefore, the LSR of pile elements to the vertical load N_p/N_0 also decreases with Δ, as shown in Figure 25. A significant reduction in N_p/N_0 can be observed when Δ < 3 m, and the opposite occurs when Δ > 3 m. It is suggested that Δ affects the behavior of the PCF significantly for the Δ < 3*d* condition, with a limited impact for the Δ > 3*d* condition.

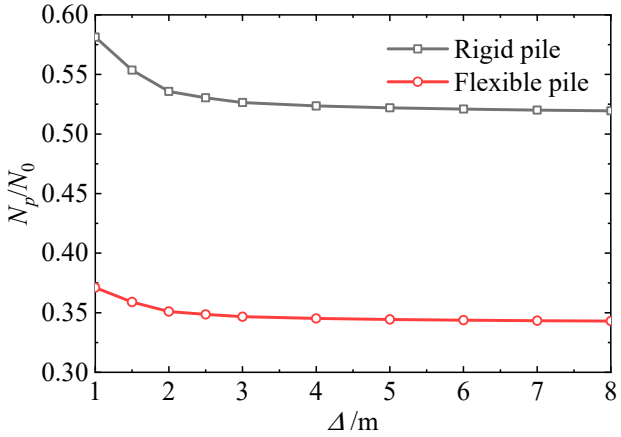


Figure 25. The LSRs of pile elements.

The overall settlement w of the PCF increases with Δ, although the N_p/N_0 is constant for the $\Delta > 3d$ condition. Therefore, the N_0/wdE_s decreases with Δ and the decrease rate of N_0/wdE_s gradually diminishes, as illustrated in Figure 26. For the rigid and flexible pile conditions, the values of the N_0/wdE_s are 22.16 and 13.48 when Δ = 1 m, and 13.13 and 10.10 when Δ = 8 m.

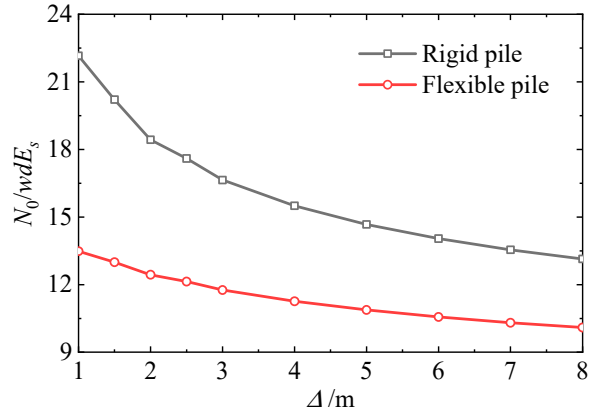


Figure 26. The N_0/wdE_s for PCF.

The effect of Δ on the differential settlement of rigid foundation w_d and the settlement of pile and soil element head w_1 is depicted in Figures 27–29. It also can be observed that (1) the settlements of the pile and soil element head w_1 increase significantly with Δ. (2) For the rigid pile condition, the settlement of rigid foundation w and the settlement of pile and soil element head w_1 exhibit a uniform settlement distribution when Δ = 1 m; the differential settlement of rigid foundation w_d increases gradually with Δ; and the counterclockwise rotation of the rigid foundation can be observed. For instance, the differential settlement between the leftmost and rightmost side soil elements reaches 7.6 mm, and the differential settlement of rigid foundation w_d reaches 9.2 mm when Δ = 8 m. (3) For the flexible pile condition, the clockwise rotation of the rigid foundation also can be seen, which means that the settlement of the long pile side is always larger than that of the short pile side when Δ = 1~8 m. The differential settlement w_d decreases with Δ. For instance, the differential settlement between the leftmost and rightmost side soil elements reaches −14.8 mm and −3.7 mm, and w_d reaches 16.7 mm and and 4.0 mm, respectively, when Δ = 1 m and Δ = 8 m.

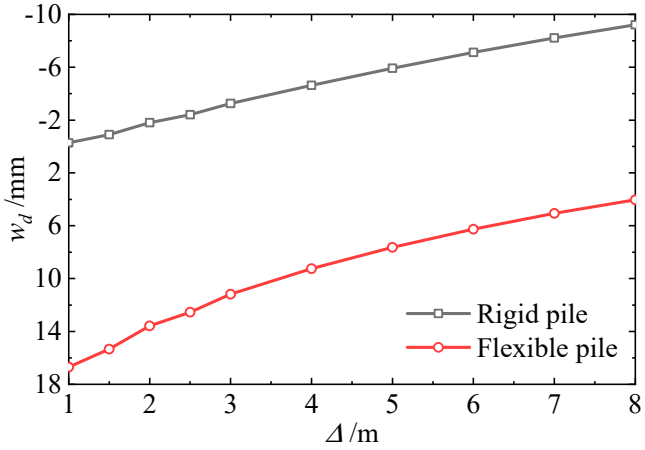


Figure 27. The differential settlement of foundation w_d.

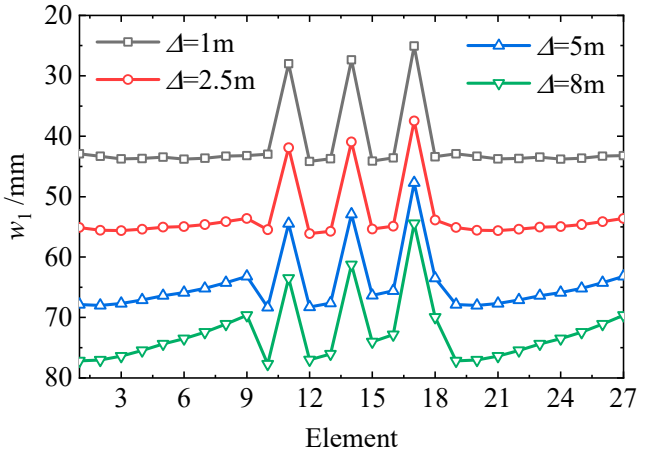


Figure 28. The settlement of pile and soil element head (rigid pile).

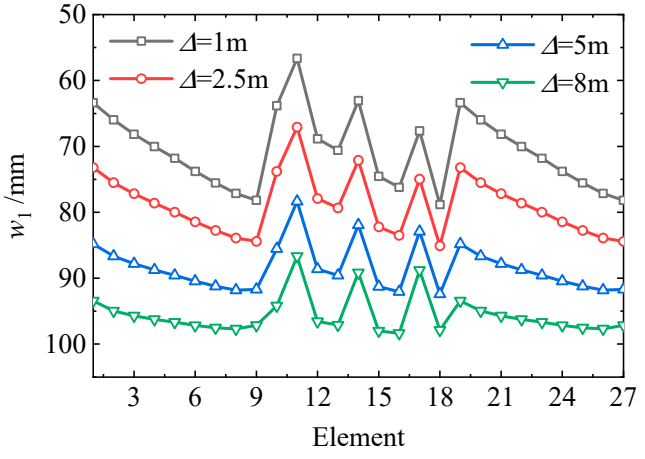


Figure 29. The settlement of pile and soil element head (flexible pile).

4.4. Effects of the Pile Length to Diameter Ratio l/d

The effects of the pile length to diameter ratio *l/d* on the bearing behaviors of the PCF proposed in Figure 9 are illustrated. The pile length of pile 2 l_2 is abbreviated as l and it is assumed that l/d = 5~21. The remaining parameters are still in line with previous configurations.

The axial force distribution of pile 1 for different *l/d* conditions is shown in Figures 30 and 31. For the rigid pile condition, (1) the axial force distribution of pile

1 is affected by l/d, as the vertical stiffness of pile 1 increases significantly with l/d. Therefore, the axial forces of the pile shaft increase significantly with l/d, and the increase rate gradually diminishes. Furthermore, the attenuation trend of the axial force along the pile shaft is consistent for different l/d conditions. (2) The neutral layer depth of pile 1 increases gradually with l/d. For instance, the neutral layer depth of pile 1 changes from 0 m to 2.4 m when l/d increases from 5 to 21. For the flexible pile condition, (1) the pile element exhibits a weaker load transfer ability along the pile shaft compared with the rigid pile condition. Therefore, the more obvious attenuation trend of the axial force for the pile element can be observed as a relatively small E_p/E_s for different l/d conditions. The increasing magnitude of the axial force of the pile element is significantly smaller than the corresponding value in the rigid pile condition. (2) The penetration of the pile head into the cushion is limited by the relatively small E_p/E_s, which results in a smaller neutral layer depth compared to the corresponding rigid pile condition. Furthermore, the ratio of the maximum axial force of the pile shaft to the pile head is also smaller. (3) The axial force of pile 1 does not increase with l/d when $l/d > 9$, which indicates that the flexible pile has reached its critical pile length, and a further increase in pile length should not affect the load transfer along the pile shaft.

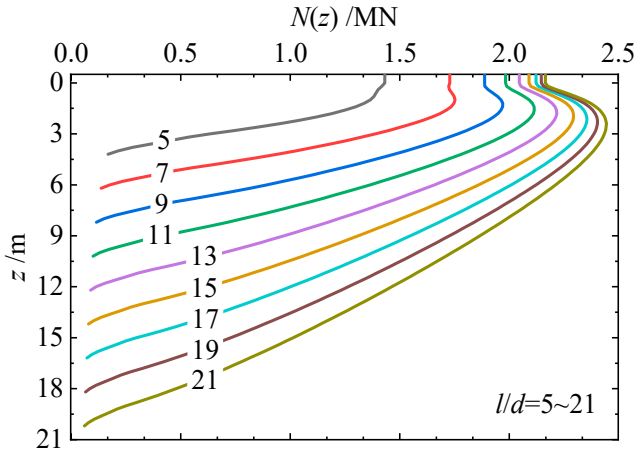


Figure 30. The differential settlement of foundation w_d.

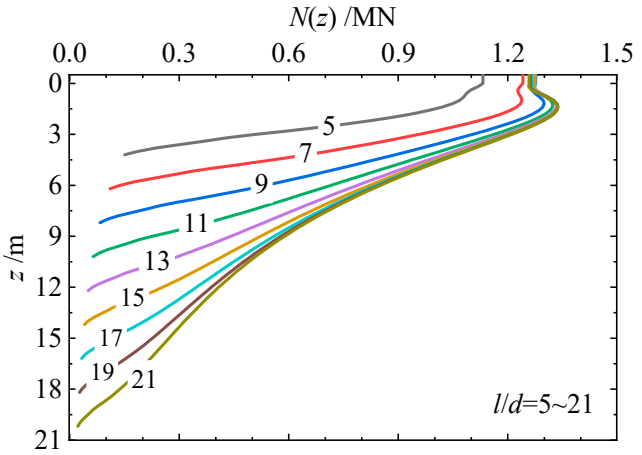


Figure 31. The settlement of pile and soil element head (rigid pile).

As depicted in Figures 32 and 33, a distinct relationship between the LSR for pile element N_i/N_0 and l/d can be observed for the different pile rigidity conditions.

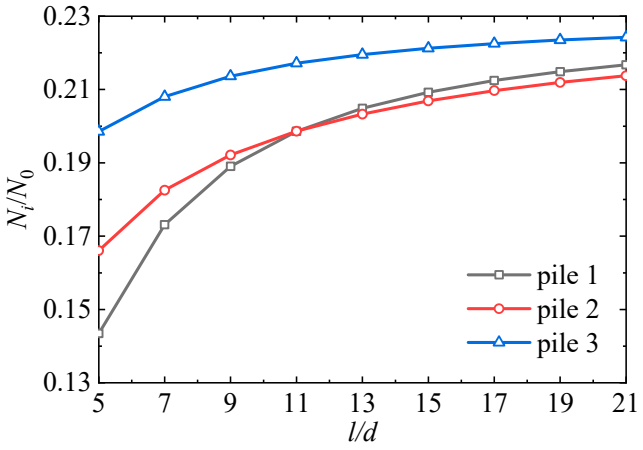


Figure 32. The LSR of each pile element (rigid pile).

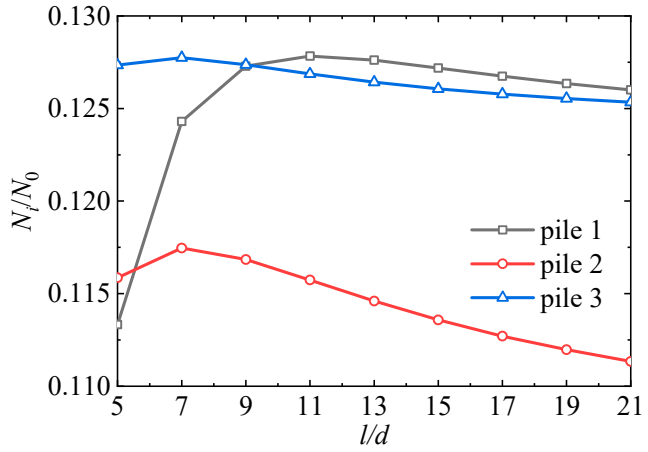


Figure 33. The LSR of each pile element (flexible pile).

For the rigid pile condition, (1) the LSR for all the pile elements increases with l/d, and the increase rate gradually diminishes. (2) The relative vertical stiffnesses of three pile elements have shown a significant difference when l/d is relatively small. The vertical stiffness difference among the piles decreases with l/d. For instance, the LSRs of pile 1, pile 2, and pile 3 are 0.143, 0.166, and 0.199, respectively, when l/d = 5, and 0.217, 0.214, and 0.224 for the l/d = 21 condition. (3) Regarding the order of the vertical stiffness of the pile element head, we have pile 1 < pile 2 < pile 3 when l/d < 11, and pile 2 < pile 1 < pile 3 when l/d > 11. The reason is that the pile length becomes the controlling factor in the vertical stiffness of the piles when l/d is relatively small, and the pile–soil interaction becomes the controlling factor in the vertical stiffness of the piles with the increase in l/d.

For flexible pile conditions, (1) the LSRs for all the pile elements increase first and then decrease with l/d. It can be interpreted that the underlying inclined bedrock plays an important role in the vertical stiffness of the pile head. The embedded depth of the inclined bedrock is shallow when l/d is relatively small; the existence of the inclined bedrock significantly changes the displacement field distribution and enhances the vertical stiffness of the pile head. (2) With the increase in l/d, the vertical stiffness of the pile head increases gradually, while the influence of the inclined bedrock on the vertical stiffness of the pile head is weakened gradually. Combining the two factors mentioned above, the vertical stiffness of the piles still increases. For instance, when l/d increases from 5 to 11, the LSR changes from 0.113 to 0.128 for pile 1, 0.116 to 0.117 for pile 2, and 0.127 to 0.1028 for pile 3. (3) The vertical behaviors of the PCF tend to be the same with a semi-infinite elastic medium, not only as the pile length difference among piles is relatively smaller compared

with the value of the pile length, but also because the influence of the inclined bedrock is smaller for the larger l/d condition. For instance, the LSRs of pile 1 and pile 3 are relatively close, and a relatively smaller LSR for pile 2 can be observed compared with the side piles when $l/d = 21$.

The N_0/wdE_s of the rigid foundation is influenced by the pile length and the embedded depth of the inclined bedrock. With the increase in l/d, the overall vertical stiffness of the PCF increases, but, on the other hand, the overall vertical stiffness of the PCF decreases with the increased embedded depth of the bedrock. As shown in Figure 34, the vertical stiffness of piles plays a controlling role in N_0/wdE_s, due to the stronger load transfer ability for piles and the weaker influence of the bedrock under rigid pile conditions. Therefore, the N_0/wdE_s increases almost linearly with the increase in l/d. Liu [45] obtained the same conclusion, namely that the pile length is the first factor that should be adjusted to reduce the settlement of the PCF. In contrast, for the flexible pile condition, the piles have shown a weaker load transfer ability, which means that the effect of l/d on the N_0/wdE_s is not notable, and the existence of the bedrock represents a controlling factor on the N_0/wdE_s. Therefore, the N_0/wdE_s gradually decreases with l/d.

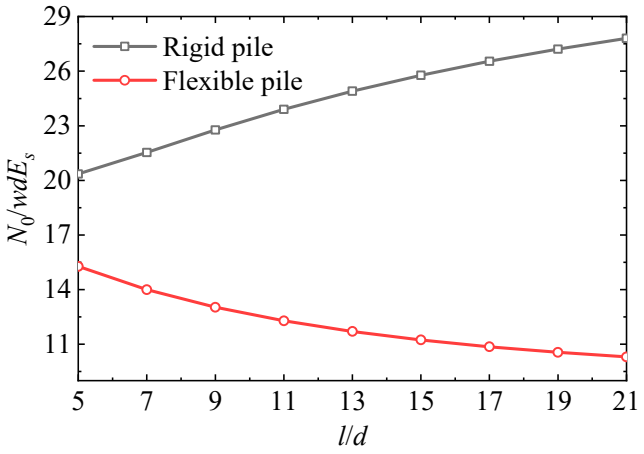


Figure 34. The N_0/wdE_s for PCF.

As shown in Figure 35, the relationship between the differential settlement w_d of the rigid foundation and l/d exhibits distinct trends for different pile rigidity conditions. It can be seen from Figure 35 that (1) the differential settlement w_d remains relatively small. The w_d changes from -0.94 mm to 2.20 mm as l/d increases from 5 to 21. (2) The differential settlement w_d decreases with l/d, and the sign of w_d is always positive, which indicates that the rigid foundation invariably experiences clockwise rotation for different values of l/d.

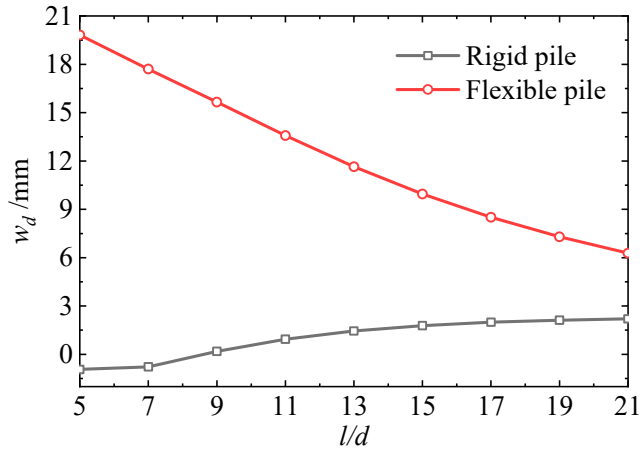


Figure 35. The differential settlement of foundation w_d.

The relationship between the settlement of the pile and soil element head w_1 and l/d is depicted in Figures 36 and 37. It can be seen that (1) w_1 is significantly affected by l/d, and w_1 decreases with l/d. However, the penetration of the pile head into the cushion is slightly affected by l/d. For the rigid pile condition, when considering l/d = 5 and l/d = 21, the w_1 of pile 3 is about 30 mm and 15 mm, respectively, and the differential settlement between pile 3 and the neighboring soil element 18 is about 17 mm and 20 mm; for the flexible pile condition, when considering l/d = 5 and l/d = 21, the w_1 of pile 3 is about 59 mm and 87 mm, respectively, and the differential settlement between pile 3 and the neighboring soil element 18 is about 13 mm and 12 mm, respectively.

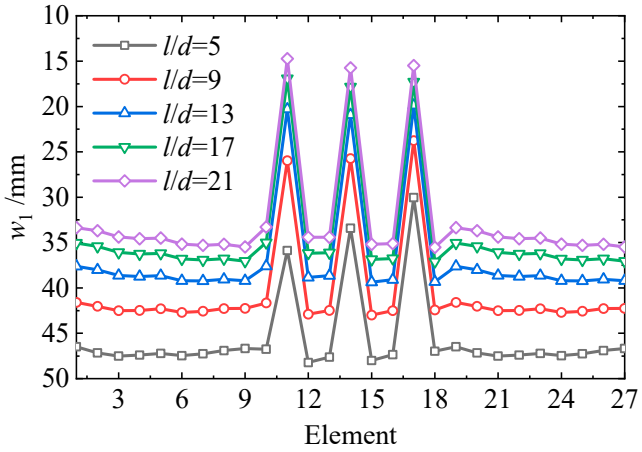


Figure 36. The settlement of pile and soil element head (rigid pile).

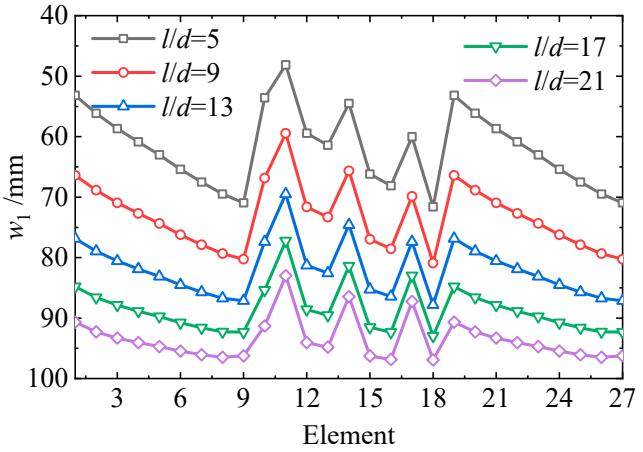


Figure 37. The settlement of pile and soil element head (flexible pile).

5. Conclusions

An integral method is proposed to study the vertical behaviors of dissimilar PCFs located over inclined bedrock. A model of dissimilar PCFs with n piles is established, and then the governing equation for the axial force along fictitious piles is established based on the boundary element method and solved with an iterative algorithm. Field load tests and FEM are introduced to validate the proposed method, and the settlement and load transfer behaviors of a 3 × 1 dissimilar PCF and its influence factors are analyzed. The main conclusions are as follows.

(1) For rigid pile conditions, rigid piles exhibit significant vertical stiffness and a strong load transfer ability. The factor of the pile length plays a controlling role in the PCF's behaviors. Therefore, regarding the axial force of the pile shaft, the N_0/wdE_s of the PCF increases with l/d, and the displacement mode of the piles is characterized as rigid body settlement. For the flexible pile condition, the LSR of the piles and the

N_0/wdE_s of the PCF are affected by the pile length and the distance from the pile bottom to bedrock Δ. Due to the relatively weaker load transfer ability of piles, the compression of the pile shaft cannot be ignored. The vertical rigidity of piles has a significant influence on the load distribution and settlement behaviors of the PCF.

(2) The depth of the neutral layer of piles decreases with an increase in the cushion stiffness. The neutral layer depth of the pile for the rigid pile condition is larger than that for the flexible pile condition when considering the same cushion stiffness. Additionally, the LSRs of the piles N_i/N_0 and the N_0/wdE_s of the PCF increase with K_c, and the average settlement and differential settlement of the rigid foundation decrease with K_c.

(3) The neutral layer depth of piles is not significantly affected by the distance from the pile bottom to bedrock Δ. The LSRs of piles decrease with Δ and increase significantly with the pile rigidity. The N_0/wdE_s of the PCF decreases with Δ, and the decrease rate gradually diminishes. The settlement of the pile and soil element head w_1 increases significantly with Δ and decreases with l/d. The differential settlement of rigid foundation w_d is affected by the pile vertical stiffness and the parameter Δ.

Although the research has described the vertical performance of dissimilar PCFs over inclined bedrock, no standards or open codes are available to analyze or design dissimilar PCFs over inclined bedrock. Therefore, more field load tests should be performed, and complete design methods for engineering should be established to promote the PCF's applications.

Author Contributions: Methodology, software, validation, Y.Z.; writing—original draft preparation, supervision, L.T. and Z.Y.; project administration, L.Y.; investigation, K.J. and X.G. All authors have read and agreed to the published version of the manuscript.

Funding: This project was supported by the General Program of the China Postdoctoral Science Foundation (2023MD734111) and sponsored by the Natural Science Foundation of Chongqing, China (CSTB2023NSCO-MSX0853, CSTB2023NSCO-MSX0433, CSTC2021JCYJ-MSXMX0343), the Scientific and Technological Research Program of Chongqing Municipal Education Commission (KJQN202101236, KJZD-K202301205, KJQN-202301260), and the Cooperation Projects between Universities of Chongqing and Institutes Affiliated to the Chinese Academy of Sciences (HZ2021012).

Data Availability Statement: The data used to support the findings of this study are available from the corresponding author upon request. The data are not publicly available due to privacy.

Conflicts of Interest: Author Yingjie Zhou was employed by the company Chongqing Wanzhou Economic-Technological Development Area Construction & Development Co., Ltd. All Authors were employed by the company No. Three Engineering Co., Ltd. of CCCC First Highway Engineering Co., Ltd. All authors declare that the research was conducted in the absence of any commercial or financial relationships that could be construed as a potential conflict of interest.

References

1. Yang, Y.; Zhang, J. Analysis of Features of Long and Short Pile Composite Foundation in High-Rise Buildings. *Soil Mech. Found. Eng.* **2022**, *59*, 92–101. [CrossRef]
2. Fatolahzadeh, S.; Mehdizadeh, R.; Nadi, B. Study of the Effect of an Inclined Bedrock on the Bearing Capacity of Shallow Foundations. *Iran. J. Sci. Technol. Trans. Civ. Eng.* **2020**, *44*, 1359–1372. [CrossRef]
3. Ding, X.; Qu, L.; Yang, J.; Wang, C. Soil vibration induced by railway traffic around a pile under the inclined bedrock condition. *Geomech. Eng.* **2021**, *24*, 143–156.
4. Jiang, K.; Gong, W.; Xu, J.; Dai, G.; Guo, X. Effects of inclined bedrock on dissimilar pile composite foundation under vertical loading. *Geomech. Eng.* **2022**, *31*, 477–488.
5. Liming, Q.; Xuanming, D.; Changjie, Z.; Chongrong, W.; Guangwei, C. Numerical and test study on vertical vibration characteristics of pile group in slope soil topography. *Earthq. Eng. Eng. Vib.* **2021**, *20*, 377–390. [CrossRef]
6. Yu, J.L.; Zhou, J.J.; Gong, X.N.; Xu, R.Q.; Li, J.Y.; Xu, S.D. Centrifuge study on behavior of rigid pile composite foundation under embankment in soft soil. *Acta Geotech.* **2020**, *16*, 1909–1921. [CrossRef]
7. Abdrabbo, F.M.; El-wakil, A.Z. Behavior of pile group incorporating dissimilar pile embedded into sand. *Alex. Eng. J.* **2015**, *54*, 175–182. [CrossRef]

8. Fu, X.; Li, J.; Liu, J.; Hu, Z.; Tang, C. Influence of Complex Hydraulic Environments on the Mechanical Properties of Pile-Soil Composite Foundation in the Coastal Soft Soil Area of Zhuhai. *Buildings* **2023**, *13*, 563. [CrossRef]
9. *GB50007-2011*; Code for Design of Building Foundation. China Architecture Publishing & Media Co., Ltd.: Beijing, China, 2012.
10. Zhang, D.M.; Huang, Z.K.; Wang, R.L.; Yan, J.Y.; Zhang, J. Grouting-based treatment of tunnel settlement: Practice in Shanghai. *Tunn. Undergr. Space Technol.* **2018**, *80*, 181–196. [CrossRef]
11. Zhang, Z.; Gong, W.; Dai, G.; Cao, X.; Zhu, Y.; Huang, H. Field Tests on Bearing Characteristics of Large-Diameter Combined Tip-and-Side Post Grouted Drilled Shafts. *Appl. Sci.* **2021**, *11*, 11883. [CrossRef]
12. Doi, T.; Murono, Y.; Zhang, F.; Hirayama, Y. In-situ horizontal cyclic loading tests on composite foundation composed of soilbags and piles. *Soils Found.* **2023**, *63*, 101327. [CrossRef]
13. Rajan, K.C.; Sharma, K.; Raychowdhury, P.; Acharya, I.P.; Burnwal, M.L.; Misra, J. State-of-the-art review of composite caisson-pile foundation (CCPF). *Appl. Ocean. Res.* **2023**, *136*, 103571.
14. Yasser, A.; Hassona, F.; Hakeem, B.M.; Moussa Abu Bakr, A. Finite element simulation of piled raft capacity under different loading conditions. *J. Adv. Eng. Trends* **2022**, *42*, 141–155. [CrossRef]
15. Ma, Q.; Mou, J.; Xiao, H. Experimental and Numerical Studies on Bearing Characteristics of Hexagonal-Section Composite Foundation Element. *Iran. J. Sci. Technol. Trans. Civ. Eng.* **2021**, *45*, 929–939. [CrossRef]
16. Saeedi Azizkandi, A.; Rasouli, H.; Baziar, M.H. Load Sharing and Carrying Mechanism of Piles in Non-connected Pile Rafts Using a Numerical Approach. *Int. J. Civ. Eng.* **2018**, *17*, 793–808. [CrossRef]
17. Huang, M.; Liang, F.; Jiang, J. A simplified nonlinear analysis method for piled raft foundation in layered soils under vertical loading. *Comput. Geotech.* **2011**, *38*, 875–882. [CrossRef]
18. Kodikara, J.K.; Johnston, I.W. Analysis of compressible axially loaded piles in rock. *Int. J. Numer. Anal. Methods Geomech.* **1994**, *18*, 427–437. [CrossRef]
19. El-Garhy, B.M. A Simplified Method for the Nonlinear Analysis of Composite Piled Raft Foundation. *Geotech. Geol. Eng.* **2022**, *40*, 4357–4375. [CrossRef]
20. Yang, M.H.; Zhang, X.W.; Zhao, M.H. A simplified approach for settlement calculation of pile groups considering pile-to-pile interaction in layered soils. *J. Cent. South Univ. Technol.* **2011**, *18*, 2131–2136. [CrossRef]
21. Kitiyodom, P.; Matsumoto, T. A simplified analysis method for piled raft and pile group foundations with batter piles. *Int. J. Numer. Anal. Methods Geomech.* **2002**, *26*, 1349–1369. [CrossRef]
22. Shen, W.Y.; Chow, Y.K.; Yong, K.Y. A variational approach for the analysis of pile group–pile cap interaction. *Geotechnique* **2000**, *50*, 349–357. [CrossRef]
23. Shen, W.Y.; Chow, Y.K.; Yong, K.Y. Variational solution for vertically loaded pile groups in an elastic half-space. *Geotechnique* **1999**, *49*, 199–213. [CrossRef]
24. Poulos, H.G.; Davis, E.H. *Pile Foundation Analysis and Design*; Wiley: New York, NY, USA, 1980.
25. Banerjee, P.K.; Davies, T.G. The behaviour of axially and laterally loaded single piles embedded in nonhomogeneous soils. *Geotechnique* **1978**, *28*, 309–326. [CrossRef]
26. Liang, F.; Chen, L.; Han, J. Integral equation method for analysis of piled rafts with dissimilar piles under vertical loading. *Comput. Geotech.* **2009**, *36*, 419–426. [CrossRef]
27. Liang, F.Y.; Song, Z. BEM analysis of the interaction factor for vertically loaded dissimilar piles in saturated poroelastic soil. *Comput. Geotech.* **2014**, *62*, 223–231. [CrossRef]
28. Chen, S.L.; Song, C.Y.; Chen, L.Z. Two-pile interaction factor revisited. *Can. Geotech. J.* **2011**, *48*, 754–766. [CrossRef]
29. Butterfield, R.; Banerjee, P.K. The Elastic Analysis of Compressible Piles and Pile Groups. *Geotechnique* **1971**, *21*, 43–60. [CrossRef]
30. Butterfield, R.; Banerjee, P.K. The Problem of Pile Group–Pile Cap Interaction. *Geotechnique* **1971**, *21*, 135–142. [CrossRef]
31. Kuwabara, F. An Elastic Analysis for Piled Raft Foundations in a Homogeneous Soil. *Soils Found.* **1989**, *29*, 82–92. [CrossRef]
32. Randolph, M.F.; Wroth, C.P. An analysis of the vertical deformation of pile groups. *Geotechnique* **1979**, *29*, 423–439. [CrossRef]
33. Lu, J.F.; Liu, Y.; Huang, Y.J.; Feng, Q.S. Dynamic response of the periodic pile-reinforced composite foundation to harmonic seismic waves. *Soil Dyn. Earthq. Eng.* **2022**, *161*, 107418. [CrossRef]
34. Hu, K.; Jiang, K.; Gou, X.; Wei, W.; Yan, L.; Zhou, T.; Guo, Z.; Chen, G. Dissimilar Pile Raft Foundation Behavior under Eccentric Vertical Load in Elastic Medium. *Buildings* **2023**, *13*, 3040. [CrossRef]
35. Xu, H.; Zhang, S.; Li, W.; Cao, Z.; Jiang, K. Behaviors and group effects of pile composite foundation under lateral load. *Results Eng.* **2023**, *17*, 100899. [CrossRef]
36. Muki, R.; Sternberg, E. Elastostatic Load-Transfer to a Half-Space from a Partially Embedded Axially Loaded Rod. *Int. J. Solids Struct.* **1970**, *6*, 69–90. [CrossRef]
37. Burmister, D.M. The General Theory of Stresses and Displacements in Layered Systems. I. *J. Appl. Phys.* **1945**, *16*, 89–94. [CrossRef]
38. Kitiyodom, P.; Matsumoto, T. A simplified analysis method for piled raft foundations in non-homogeneous soils. *Int. J. Numer.* **2003**, *27*, 85–109. [CrossRef]
39. Poulos, H.G. Stresses and displacements in an elastic layer underlain by a rough rigid base. *Geotechnique* **1967**, *17*, 378–410. [CrossRef]
40. Zhang, L.; Wang, T.; Zhao, Z.; Jin, X. Research on Bearing Difference between Single-Pile Composite Foundation Field Test and Group-Pile Composite Foundation of High-Rise Buildings. *Buildings* **2023**, *13*, 2127. [CrossRef]

41. Song, H.L.; Zhao, R.F.; Zhao, G.T. Calculation method for composite modulus of flexible pile composite foundation for high-speed railway under post-work settlement source. *Constr. Build. Mater.* **2024**, *411*, 134576. [CrossRef]
42. Halder, P.; Manna, B. Large scale model testing to investigate the influence of granular cushion layer on the performance of disconnected piled raft system. *Acta Geotech.* **2021**, *16*, 1597–1614. [CrossRef]
43. Malekkhani, M.J.; Bazaz, J.B. An Analytical Model to Study the Behavior of Non-connected Piled Rafts with Granular Cushion Subjected to Vertical Load. *Int. J. Civ. Eng.* **2021**, *19*, 941–956. [CrossRef]
44. Yang, Y.; Cheng, Y.P.; Gong, W.; Fan, H.; Dai, G. Effect of cushion types on the seismic response of structure with disconnected pile raft foundation. *Structures* **2023**, *48*, 1333–1345. [CrossRef]
45. Liu, S.; Guo, P.; Li, X.; Wang, K.; Tang, R.; Wang, Y. Settlement Behavior of Composite Foundation with Deep Mixed Piles Supporting Highway Subgrades in Water-Rich Flood Plains. *Water* **2023**, *15*, 2048. [CrossRef]

Disclaimer/Publisher's Note: The statements, opinions and data contained in all publications are solely those of the individual author(s) and contributor(s) and not of MDPI and/or the editor(s). MDPI and/or the editor(s) disclaim responsibility for any injury to people or property resulting from any ideas, methods, instructions or products referred to in the content.